

Very Light CP-odd Higgs bosons of the NMSSM at the LHC in $4b$ -quark final states

M. M. Almarashi and S. Moretti

*School of Physics & Astronomy,
University of Southampton, Southampton, SO17 1BJ, UK*

Abstract

We study the detectability of the lightest CP-odd Higgs boson of the NMSSM, a_1 , at the LHC through its production in association with a bottom-quark pair followed by the $a_1 \rightarrow b\bar{b}$ decay. It is shown that, for large $\tan\beta$ and very high luminosity of the LHC, there exist regions of the NMSSM parameter space that can be exploited to detect the a_1 through this channel. This signature is a characteristic feature of the NMSSM in comparison to the MSSM, as a_1 masses involved are well below those allowed in the MSSM for the corresponding CP-odd Higgs state.

1 Introduction

Supersymmetry (SUSY) is one of the preferred candidates for physics beyond the Standard Model (SM). The simplest version of SUSY is the Minimal Supersymmetric Standard Model (MSSM). This realisation however suffers from two critical flaws: the μ -problem and the little hierarchy problem. The former one results from the fact that the superpotential has a dimensional parameter, μ (the so-called ‘Higgs(ino) mass parameter’), that, due to SUSY, its natural values would be either 0 or the Plank mass scale; yet, phenomenologically, in order to achieve Electro-Weak Symmetry Breaking (EWSB), it is required to take values of order of the EW scale, 100 GeV, or, possibly, up to the TeV range. The latter one emerges from LEP, which failed to detect a light CP-even Higgs boson, thereby imposing severe constraints on a SM-like Higgs boson mass, 114 GeV being its lower limit from data, thereby requiring unnaturally large higher order corrections from both the SM and SUSY particle spectrum (chiefly, from third generation quarks and squarks) in order to pass such experimental constraints (recall that at tree level the lightest CP-even Higgs boson mass of the MSSM is less than M_Z).

The simplest SUSY realisation beyond the MSSM which can solve these two problems at once is the Next-to-Minimal Supersymmetric Standard Model (NMSSM) [1]. This model includes a singlet superfield in addition to the two MSSM-type Higgs doublets, giving rise to seven Higgs bosons: three CP-even Higgses $h_{1,2,3}$ ($m_{h_1} < m_{h_2} < m_{h_3}$), two CP-odd Higgses $a_{1,2}$ ($m_{a_1} < m_{a_2}$) and a pair of charged Higgses h^\pm . When the scalar component of the singlet superfield acquires a Vacuum Expectation Value (VEV), an ‘effective’ μ -term, μ_{eff} , will be automatically generated and can rather naturally have values of order of the EW/TeV scale, as required. Moreover, the NMSSM can solve the little hierarchy problem as well, or at least alleviate it greatly, in two ways: firstly, a SM-like Higgs boson can unconventionally decay into two a_1 ’s with $m_{a_1} < 2m_b$ [2], thus avoiding current Higgs bounds (yet this mass region is highly constrained by ALEPH [3] and BaBar [4] data); secondly, a CP-even Higgs (h_1 or h_2) has naturally reduced couplings to the Z boson due to the additional Higgs singlet field of the NMSSM and the ensuing mixing with the Higgs doublets.

One of the primary goals of present and future colliders is looking for Higgs bosons. In regard to the Higgs sector of the NMSSM, there has been some work dedicated to explore the detectability of at least one Higgs boson at the Large Hadron Collider (LHC) and the Tevatron. In particular, some efforts have been made to extend the so-called ‘no-lose theorem’ of the MSSM – stating that at least one Higgs boson of the MSSM should be found at the LHC via the usual SM-like production and decay channels throughout the entire MSSM parameter space [5] – to the case of the NMSSM [6, 7, 8]. By assuming that Higgs-to-Higgs decays are not allowed, it was realised that at least one Higgs boson of the NMSSM will be discovered at the LHC. However, this theorem could be violated if Higgs-to-SUSY particle decays are kinematically allowed (e.g., into neutralino pairs, yielding invisible Higgs signals) [9, 10].

So far, there is no conclusive evidence that the ‘no-lose theorem’ can be confirmed in the context of the NMSSM. In order to establish the theorem for the NMSSM, Higgs-to-Higgs decay should be taken into account, in particular $h_1 \rightarrow a_1 a_1$. Such a decay can in fact be dominant in large regions of NMSSM parameter space, for instance, for small A_k [11], and may not give Higgs signals with sufficient significance at the LHC.

Besides, there have also been some attempts to distinguish the NMSSM Higgs sector from the MSSM one, by affirming a so-called ‘more-to-gain theorem’ [12, 13, 14, 11, 15]. That is, to assess whether there exist some areas of the NMSSM parameter space where more and/or different Higgs bosons can be discovered at the LHC compared with what is expected from the MSSM. Some comparisons between NMSSM and MSSM phenomenology, specifically in the Higgs sectors of the two SUSY realisations, can be found in [16].

In this analysis, we explore the two theorems at once through studying the direct production of a very light a_1 (with $m_{a_1} < M_Z$) in association with b -quark pairs followed by the $a_1 \rightarrow b\bar{b}$ decay, hence a $4b$ -quark final state, at the LHC. This channel has a very large cross section at large $\tan\beta$ yet, being a totally hadronic signal, is plagued by very large (both reducible and irreducible) backgrounds.

This work is complementary to the one carried in [11, 15], in which we explored the $\tau^+\tau^-$, $\gamma\gamma$ and $\mu^+\mu^-$ decay modes of such a light a_1 state (again, produced in association with b -quark pairs).

This paper is organised as follows: in Sec. 2, we describe the parameter space scan performed and give inclusive event rates for the signal. In Sec. 3, we analyse signal and QCD backgrounds for some benchmark points. Finally, we summarise and conclude in Sect. 4.

2 Parameter Scan and Inclusive Signal Rates

In our exploration of the Higgs sector of the NMSSM, we used here the fortran package NMSSMTools developed in Refs. [17, 18]. This package computes the masses, couplings and decay rates (widths and Branching Ratios (BRs)) of all the Higgs bosons of the NMSSM in terms of its parameters at the EW scale. NMSSMTools also takes into account theoretical as well as experimental constraints from negative Higgs searches at LEP [19] and the Tevatron¹, along with the unconventional channels relevant for the NMSSM.

The features of the scan performed have been already discussed in Refs. [11, 15], to which we refer the reader for details. We map the NMSSM parameter space in terms of six independent input quantities: the Yukawa couplings λ and κ , the soft trilinear terms A_λ and A_κ , plus $\tan\beta$ (the ratio of the VEVs of the two Higgs doublets) and $\mu_{\text{eff}} = \lambda\langle S \rangle$ (where $\langle S \rangle$ is the VEV of the Higgs singlet).

For successful data points generated in the scan, i.e., those that pass both theoretical and experimental constraints, we used CalcHEP [20] to determine the cross-sections for NMSSM Higgs production². As the SUSY mass scales have been arbitrarily set well above the EW one (see Refs. [11, 15]), the NMSSM Higgs production modes exploitable in simulations at the LHC are those involving couplings to heavy ordinary matter only. Amongst the production channels onset by the latter, we focus here on $gg, q\bar{q} \rightarrow b\bar{b} a_1$, i.e., Higgs production in association with a b -quark pair. This production mode is the dominant one at large $\tan\beta$. We chose $gg, q\bar{q} \rightarrow b\bar{b} a_1 \rightarrow b\bar{b} b\bar{b}$ also because b -tagging can be exploited to trigger on the signal and enable us to require four displaced vertices in order to reject light jets. The ensuing $4b$ signature (in which we do not enforce a charge measurement) has already been exploited to detect neutral Higgs bosons of the MSSM at the LHC and proved useful, provided $\tan\beta$ is large and the collider has good efficiency and purity in tagging b -quark jets, albeit for the case of rather heavy Higgs states (with masses beyond M_Z , typically) [22, 23].

As an initial step of the analysis, we have computed the fully inclusive signal production cross-section times the decay BR against each of the six parameters of the NMSSM. Figs. 1 and 2 present the results of our scan, the first series of plots (in Fig. 1) illustrating the distribution of event rates over the six NMSSM parameters plus as a function of the BR and of m_{a_1} . The plots in Fig. 2 display instead the correlations between the $a_1 \rightarrow b\bar{b}$ decay rate versus the a_1 mass and the $a_1 \rightarrow \gamma\gamma$ decay rate. It is clear from Fig. 1 that, for our parameter space, the large $\tan\beta$ and small μ_{eff} (and, to some extent, also small λ) region is the one most compatible with current theoretical and experimental constraints, while the distributions in κ , A_λ and A_κ are rather uniform (top six panes in Fig. 1). From a close look

¹Speculations of an excess at LEP which could be attributed to NMSSM Higgs bosons are found in [2].

²We adopt herein CTEQ6L [21] as parton distribution functions, with scale $Q = \sqrt{s}$, the centre-of-mass energy at parton level, for all processes computed.

at the bottom-left pane of Fig. 1, it is further clear that the $\text{BR}(a_1 \rightarrow b\bar{b})$ is dominant for most points in the parameter space, about 90% and above. In addition, by looking at the the bottom-right pane of Fig. 1, it is remarkable to notice that the event rates are sizable in most regions of parameter space, topping the 10^7 fb level for small values of m_{a_1} and are decreasing rapidly with increasing m_{a_1} . However, there are some points in parameter space, with m_{a_1} between 40 to 120 GeV, as shown in the left pane of Fig. 2, in which the $\text{BR}(a_1 \rightarrow b\bar{b})$ is reduced due to the enhancement of the $\text{BR}(a_1 \rightarrow \gamma\gamma)$ (see right pane of the same figure), phenomenon peculiar to the NMSSM and which depends upon the amount of Higgs singlet-doublet mixing, see [11].

3 Signal-to-Background Analysis

We perform here a partonic signal-to-background (S/B) analysis, based on CalcHEP results. We assume $\sqrt{s} = 14$ TeV throughout for the LHC energy. We apply the following cuts in our calculations:

$$\Delta R(j, j) > 0.4, \quad |\eta(j)| < 2.5, \quad P_T(j) > 15 \text{ GeV}. \quad (1)$$

Here, we assume that the b -tagging probability of a b -quark is 50% while the mis-tagging probability of a gluon is 1% and the one for a light quark is 2%. Figs. 3-7 show the distributions of the invariant mass of a two b -jet (di-jet) system after multiplying the production times decay rates (after cuts) by the aforementioned efficiency/rejection factors, i.e., true b -tagging and mis-tagging probability. It is clear that the largest background is the irreducible one $b\bar{b}b\bar{b}$, which is one order of magnitude larger than the reducible background $b\bar{b}gg$. Further, the other reducible background, involving light quarks, labelled here as $b\bar{b}c\bar{c}$, is negligible compared to the other two. Notice that all these backgrounds reach their maximum in invariant mass at around 40 GeV. Our plots have a bin width of 1 GeV and account for all combinatorial effects (as appropriate in absence of jet-charge determination).

To claim discovery of the lightest CP-odd Higgs, a_1 , at the LHC, we plotted in Fig. 8 both signal significances, left-panes, and corresponding signal event rates, right-panes, as a function of the collected luminosity, and after integrating over 10 and 5 bins (thus mimicking a more optimistic and a more conservative, respectively, detector resolution in mass of a di-jet system). From this figure, there is a small window to detect a_1 with masses between 35 at 50 GeV at a very large luminosity, $L = 300 \text{ fb}^{-1}$, which could well pertain to the final number of recorded events of the LHC at design luminosity. Further, for an upgraded LHC, with a tenfold increase in design luminosity, known as the Super-LHC (SLHC), which could well lead to data sample with $L = 1000 \text{ fb}^{-1}$, there is clear potential to detect an a_1 with mass up to 80 GeV or so. This is the more probable the better the experimental resolution, naturally.

Finally, notice in Figs. 9-10 the distributions in pseudorapidity-azimuth (the standard cone measure) separation of di-jet pairs and average transverse momentum of the jets, respectively (in the latter case we also distinguish, in the reducible backgrounds, between b -jets and non- b -jets, by exploiting our knowledge of the Monte Carlo ‘truth’). Guided by Refs. [22, 23], this has been done to check whether further cuts (in addition to those in eq. (1))

could be employed to improve the chances of detecting these particular final states. While some combinations of cuts in these quantities are more efficient for the signal than the backgrounds, there is no overall gain in the signal significance, further, to the cost of a reduced signal absolute rate. (Results are here shown for just one signal mass value, yet they are typical also for the other masses considered too.)

4 Conclusions

The Higgs sector of the NMSSM is phenomenologically richer than the one of the MSSM as it has two more (neutral) Higgs states. In this paper, we explored the detectability of the lightest CP-odd Higgs state of the NMSSM, a_1 , at the LHC and SLHC, through its production in association with a $b\bar{b}$ pair followed by $a_1 \rightarrow b\bar{b}$ decay. We have shown that there are some regions of NMSSM parameter space where a rather light a_1 state can be discovered at very large integrated luminosity using standard reconstruction techniques [24, 25]. This is true so long that $\tan\beta$ is very large, typically above 30, over an m_{a_1} interval extending from 20 GeV to 80 GeV, depending on the collider configuration. High b -tagging efficiency is crucial to achieve this, to transverse momenta as low as 15 GeV, ideally, also accompanied by di-jet mass resolutions up to 10 GeV.

Firstly, these results (together with those of Refs.[11, 15]) support the ‘no-lose theorem’ by looking for the (quite possibly resolvable) direct production of a light a_1 rather than looking for its production through the decay $h_{1,2} \rightarrow a_1 a_1$, whose detectability remains uncertain. Secondly, they enable distinguishing the NMSSM Higgs sector from MSSM one (thus contributing to enforcing a ‘more-to-gain theorem’) since such light CP-odd Higgs states, below M_Z (which have a large singlet component), are not at all possible in the context of the MSSM.

In reaching these conclusions we have, first, sampled the entire parameter space of the NMSSM to extract the regions which are interesting phenomenologically and, then, sampled five benchmark points in the NMSSM parameter space (see the captions to Figs. 3-7), all taken at large $\tan\beta$, for which we have extracted the detector performances and collider luminosities required for discovery. The encouraging results obtained should help to motivate further and more detailed analyses.

Acknowledgments

This work is supported in part by the NExT Institute. M. M. A. acknowledges a scholarship granted to him by Taibah University (Saudi Arabia).

References

- [1] For reviews, see: e.g., U. Ellwanger, C. Hugonie and A. M. Teixeira, Phys. Rept. **496** (2010) 1 (and references therein); M. Maniatis, Int. J. Mod. Phys. A **25** (2010) 3505 (and references therein).
- [2] R. Dermisek and J. F. Gunion, Phys. Rev. D **76** (2007) 095006.
- [3] S. Schael *et al.* [ALEPH Collaboration], JHEP **1005** (2010) 049.
- [4] B. Aubert *et al.* [BABAR Collaboration], Phys. Rev. Lett. **103** (2009) 181801.
- [5] J. Dai, J.F. Gunion, R. Vega, Phys. Lett. B **315** (1993) 355 and Phys. Lett. B **345** (1995) 29; J.R. Espinosa, J.F. Gunion, Phys. Rev. Lett. **82** (1999) 1084.
- [6] U. Ellwanger, J. F. Gunion and C. Hugonie, JHEP **0507** (2005) 041; U. Ellwanger, J.F. Gunion, C. Hugonie and S. Moretti, hep-ph/0305109 and hep-ph/0401228.
- [7] U. Ellwanger, J.F. Gunion and C. Hugonie, hep-ph/0111179; D.J. Miller and S. Moretti, hep-ph/0403137; C. Hugonie and S. Moretti, hep-ph/0110241; A. Belyaev, S. Hesselbach, S. Lehti, S. Moretti, A. Nikitenko and C. H. Shepherd-Themistocleous, arXiv:0805.3505 [hep-ph]; J. R. Forshaw, J. F. Gunion, L. Hodgkinson, A. Papaefstathiou and A. D. Pilkington, JHEP **0804** (2008) 090; A. Belyaev, J. Pivarski, A. Safonov, S. Senkin and A. Tatarinov, Phys. Rev. D **81** (2010) 075021.
- [8] S. Moretti, S. Munir and P. Poulose, Phys. Lett. B **644** (2007) 241.
- [9] U. Ellwanger and C. Hugonie, Eur. Phys. J. C **25** (2002) 297.
- [10] A. Djouadi *et al.*, JHEP **0807** (2008) 002.
- [11] M. Almarashi and S. Moretti, Eur. Phys. J. C **71** (2011) 1618.
- [12] S. Moretti and S. Munir, Eur. Phys. J. C **47** (2006) 791.
- [13] S. Munir, talk given at the ‘International School of Subnuclear Physics, 43rd Course’, Erice, Italy, August 29 – Sept. 7, 2005, to be published in the proceedings, preprint SHEP-05-37, October 2005.
- [14] E. Accomando *et al.*, arXiv:hep-ph/0608079.
- [15] M. M. Almarashi and S. Moretti, Phys. Rev. D **83** (2011) 035023.
- [16] F. Mahmoudi, J. Rathsman, O. Stal and L. Zeune, Eur. Phys. J. C **71** (2011) 1608.
- [17] U. Ellwanger, J.F. Gunion and C. Hugonie, JHEP **0502** (2005) 066; U. Ellwanger and C. Hugonie, Comput. Phys. Commun. **175** (2006) 290.
- [18] See <http://www.th.u-psud.fr/NMHDECAY/nmssmtools.html>.

- [19] S. Schael *et al.*, Eur. Phys. J. C **47** (2006) 547.
- [20] A. Pukhov, arXiv:hep-ph/0412191.
- [21] See <http://hep.pa.msu.edu/cteq/public/cteq6.html>.
- [22] J. Dai, J. F. Gunion and R. Vega, Phys. Lett. B **345** (1995) 29.
- [23] J. Dai, J. F. Gunion and R. Vega, Phys. Lett. B **387** (1996) 801.
- [24] ATLAS Collaboration, arXiv:0901.0512 [hep-ex].
- [25] CMS Collaboration, J. Phys. G **34** (2007) 995.

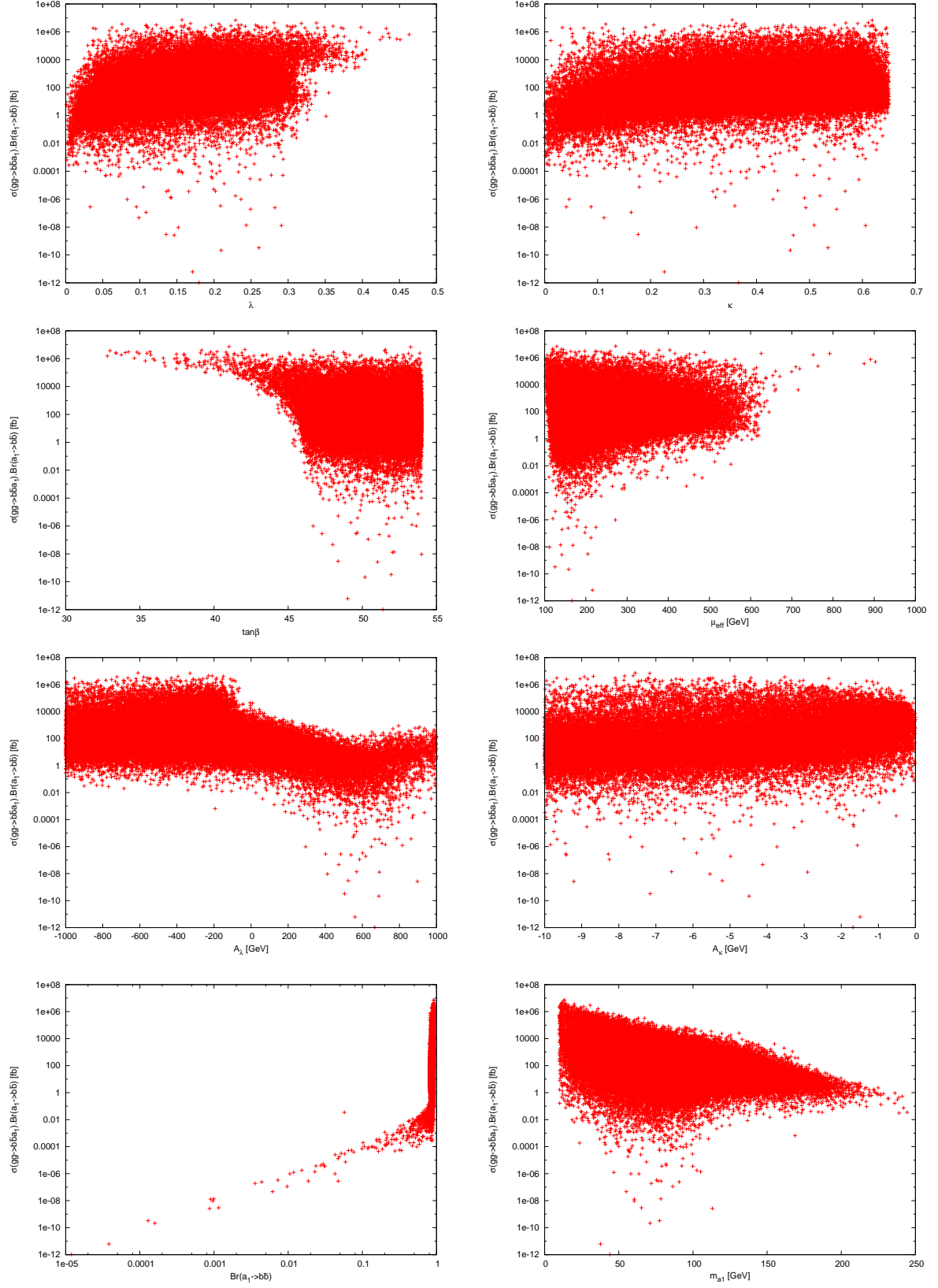


Figure 1: The rates for $\sigma(gg \rightarrow b\bar{b}a_1) \text{BR}(a_1 \rightarrow b\bar{b})$ as a function of λ , κ , $\tan\beta$, μ_{eff} , A_λ , A_κ , $\text{Br}(a_1 \rightarrow b\bar{b})$ and m_{a_1} .

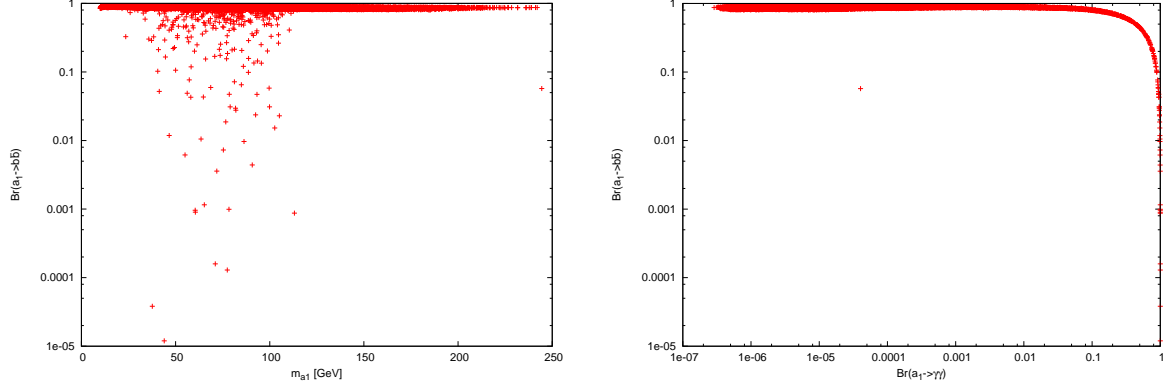


Figure 2: The $BR(a_1 \rightarrow b\bar{b})$ as a function of the CP-odd Higgs mass m_{a_1} and of the $BR(a_1 \rightarrow \gamma\gamma)$.

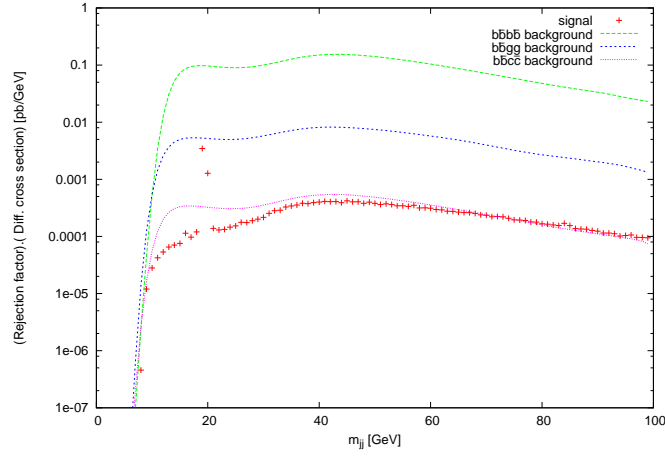


Figure 3: The differential cross-section in di-jet invariant mass m_{jj} , after the cuts in (1), for signal (with $m_{a_1}=19.98$ GeV) and backgrounds, the former obtained for the benchmark point with $\lambda = 0.075946278$, $\kappa = 0.11543578$, $\tan\beta = 51.507125$, $\mu = 377.4387$, $A_\lambda = -579.63592$ and $A_\kappa = -3.5282881$.

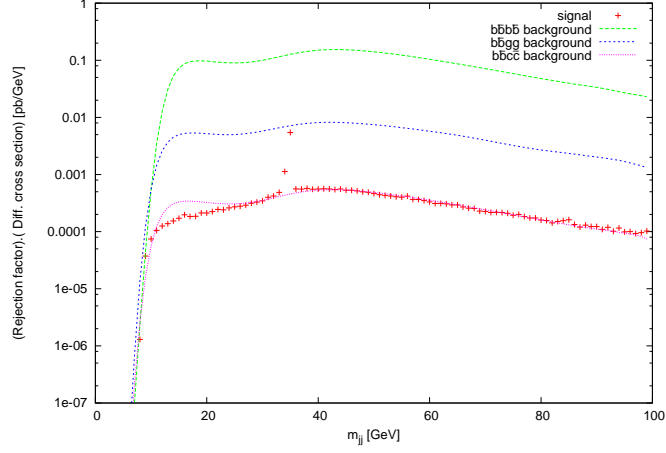


Figure 4: The differential cross-section in di-jet invariant mass m_{jj} , after the cuts in (1), for signal (with $m_{a_1}=35.14$ GeV) and backgrounds, the former obtained for the benchmark point with $\lambda = 0.091741231$, $\kappa = 0.51503049$, $\tan\beta = 38.09842$, $\mu = 130.56601$, $A_\lambda = -720.88387$ and $A_\kappa = -5.3589352$.

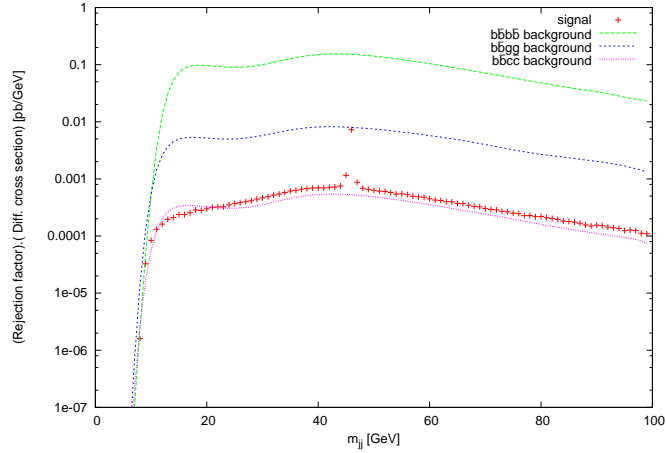


Figure 5: The differential cross-section in di-jet invariant mass m_{jj} , after the cuts in (1), for signal (with $m_{a_1}=46.35$ GeV) and backgrounds, the former obtained for the benchmark point with $\lambda = 0.14088263$, $\kappa = 0.25219468$, $\tan\beta = 50.558484$, $\mu = 317.07532$, $A_\lambda = -569.60665$ and $A_\kappa = -8.6099538$.

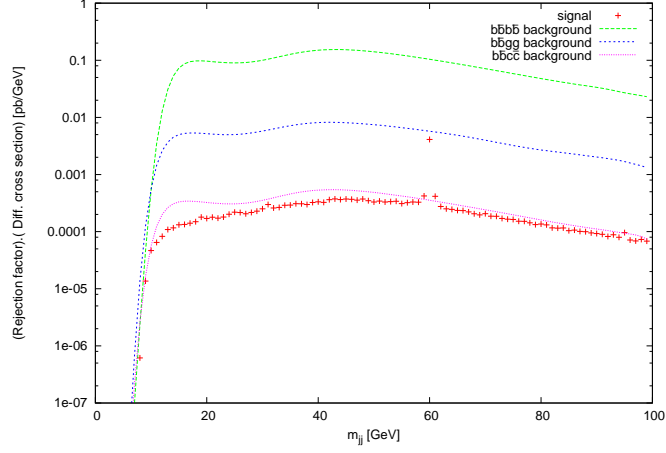


Figure 6: The differential cross-section in di-jet invariant mass m_{jj} , after the cuts in (1), for signal (with $m_{a_1}=60.51$ GeV) and backgrounds, the former obtained for the benchmark point with $\lambda = 0.17410656$, $\kappa = 0.47848034$, $\tan\beta = 52.385408$, $\mu = 169.83139$, $A_\lambda = -455.85097$ and $A_\kappa = -9.0278415$.

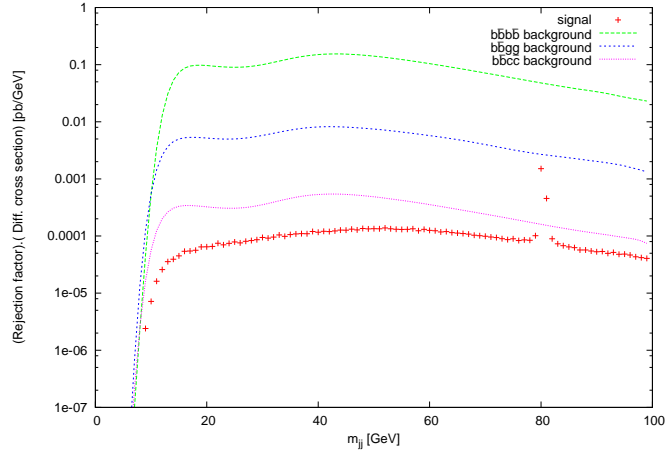


Figure 7: The differential cross-section in di-jet invariant mass m_{jj} , after the cuts in (1), for signal (with $m_{a_1}=80.91$ GeV) and backgrounds, the former obtained for the benchmark point with $\lambda = 0.10713292$, $\kappa = 0.13395171$, $\tan\beta = 44.721569$, $\mu = 331.43456$, $A_\lambda = -418.13018$ and $A_\kappa = -9.7077267$.

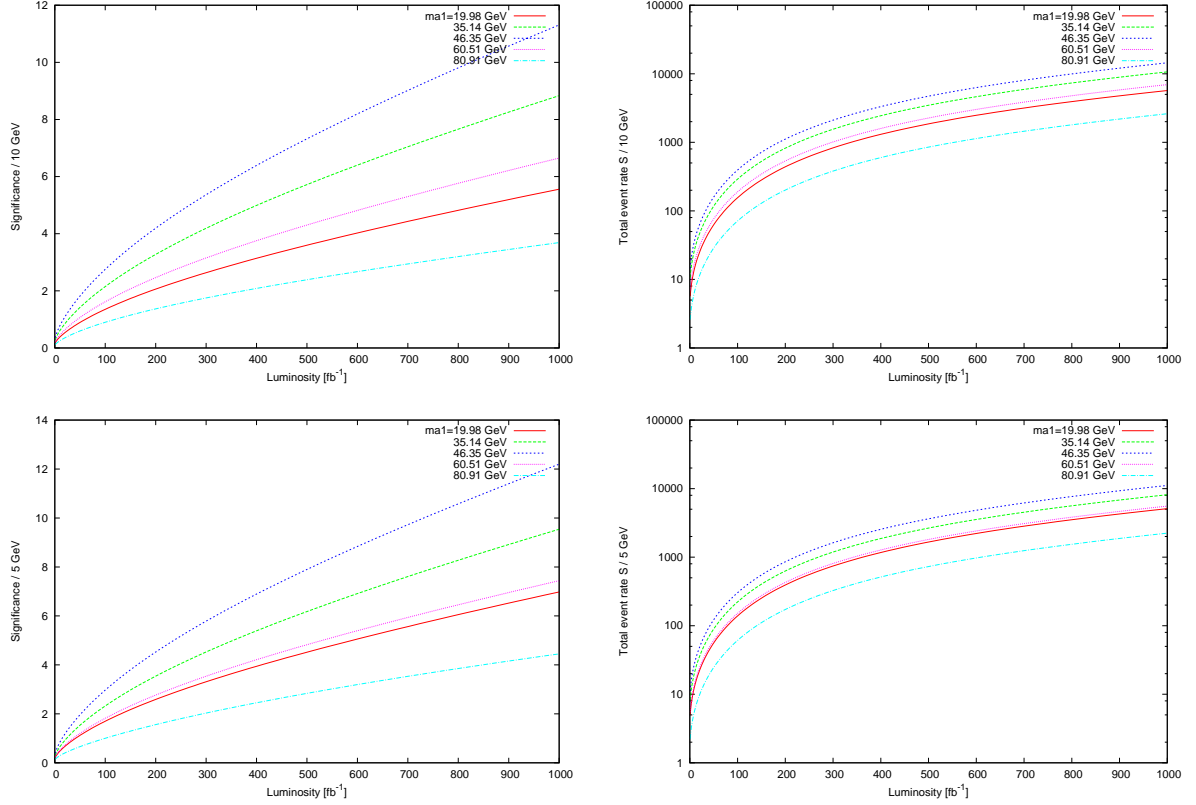


Figure 8: The significances S/\sqrt{B} (left) and total event rates S (right) of the $gg, q\bar{q} \rightarrow b\bar{b}a_1 \rightarrow b\bar{b}b\bar{b}$ signal as functions of the integrated luminosity for 10 GeV (top) and 5 GeV (bottom) di-jet mass resolutions.

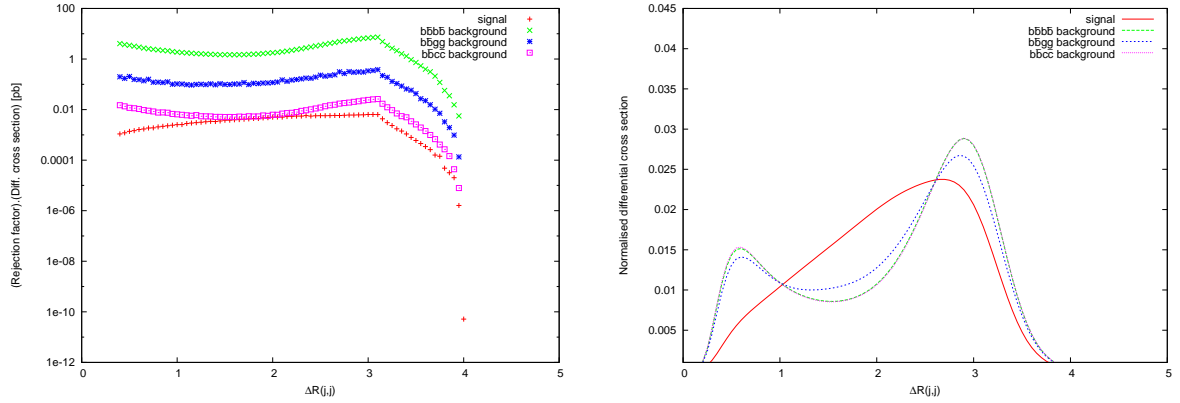


Figure 9: The differential cross-section in di-jet (pseudorapidity-azimuth) separation, after the cuts in (1), for signal (with $m_{a_1}=46.35$ GeV) and backgrounds, the former obtained for the benchmark point with $\lambda = 0.14088263$, $\kappa = 0.25219468$, $\tan\beta = 50.558484$, $\mu = 317.07532$, $A_\lambda = -569.60665$ and $A_\kappa = -8.6099538$. On the left the absolute normalisations are given while on the right those to 1.

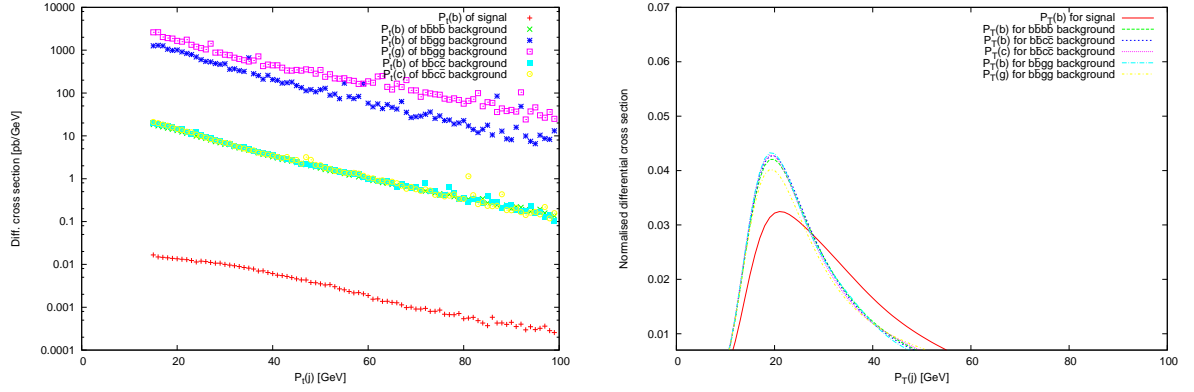


Figure 10: The differential cross-section in jet transverse momentum, after the cuts in (1), for signal (with $m_{a_1}=46.35$ GeV) and backgrounds, the former obtained for the benchmark point with $\lambda = 0.14088263$, $\kappa = 0.25219468$, $\tan\beta = 50.558484$, $\mu = 317.07532$, $A_\lambda = -569.60665$ and $A_\kappa = -8.6099538$. On the left the absolute normalisations are given while on the right those to 1.